Mapping the Nanoscale Charge Traps in Grain Structures of Indium Tin Oxide (ITO) Thin Films

Hyesong Jeon

Supervised by
Professor Miyoung Kim

A Dissertation Submitted to the Faculty of
Seoul National University
in Partial Fulfillment of the Requirements for the Degree of
Master of Engineering

February 2021

Department of Materials Science and Engineering
Graduate School
Seoul National University

공학석사 학위논문

Mapping the Nanoscale Charge Traps in Grain Structures of Indium Tin Oxide (ITO) Thin Films

ITO 박막의 결정 구조에서 나노 스케일의 전하 트랩의 매핑에 관한 연구

2021년 2월

서울대학교 대학원

재료공학부

전 혜 송

Mapping the Nanoscale Charge Traps in Grain Structures of Indium Tin Oxide (ITO) Thin Films

(ITO 박막의 결정 구조에서 나노 스케일의 전하 트랩의 매핑에 관한 연구)

지도 교수 김 미 영

이 논문을 공학석사 학위논문으로 제출함
2021년 2월

서울대학교 대학원
재료공학부
전 혜 송

전혜송의 공학석사 학위논문을 인준함
2021년 2월

위 원 장 김 상 국 (인)
부위원장 김 미 영 (인)
위 원 홍 승 훈 (인)

Abstract

Mapping the Nanoscale Charge Traps in Grain Structures of Indium Tin Oxide (ITO) Thin Films

Hyesong Jeon

Department of Materials Science and Engineering

The Graduate School

Seoul National University

Indium Tin Oxide (ITO) thin film is a highly n-doped semiconductor which has a low electrical resistivity and a high mobility. And, it shows high optical transmittances in the visible and near-IR regions. Due to these remarkable electrical and optical properties, ITO thin films have been extensively used as promising transparent conducting electrodes in many optoelectronic devices such as solar cells, light emitting diodes (LEDs), touch screen displays and so on. In applying ITO thin films as electrodes for optoelectronic devices, high electrical conductivity and electrical noise properties of ITO thin films are important factors. Meanwhile, electrical noise is an undesirable fluctuation of current signals, which deteriorates the electrical properties of electronic devices. Since the electrical noise affects the performance of nano-devices, it has to be well controlled and analyzed.

In this dissertation, we will discuss nanoscale distributions of charge traps in the grain structures of an ITO thin film, using a noise microscopy based on a conducting atomic force microscopy (C-AFM). Here, we measured the current and electrical noise maps of an ITO thin film. Using these maps, we calculated the sheet conductance and effective charge trap density maps. We identified that a sheet conductance was determined by a charge trap density in an ITO thin film. Also, we found that charge carriers transported through the localized charge traps (diffusive transport). Additionally, when we treated the ITO thin film by an oxygen plasma, a sheet conductance increased, and a charge trap density decreased. It is worth noting that remarkable changes in grain boundaries were observed, which originated from numerous defects concentrated in boundaries. Further, we revealed that charge conduction was dominated by hopping in these grain boundaries.

This work provides the important information about the effects of the activities of charge traps on charge transports in the ITO thin film, which can be a useful tool for noise studies and the enhanced performance of optoelectronic devices based on ITO electrodes.

Keywords:

ITO thin film, Electrical Noise, Charge Trap, Atomic force microscopy, Noise Microscopy, Oxygen plasma

Student Number: 2019-23053

Table of Contents

List of Figures

Chapter 1.

Introduction

1.1 Electrical Noise

Electrical noise is undesirable fluctuations of current signals, which deteriorates the electrical properties of electronic devices. The properties of electrical noises are analyzed by noise power spectral density (PSD) spectra. Noise spectra provide numerous information about the motion of charge carriers or structures of materials. [1] Also, depending on the scaling behavior of noise spectra, various kinds of noises are distinguished, such as white noise, generation-recombination (G-R) noise, and 1/f noise. [1,2] Since the electrical noise affects the performance of nano-devices [2], it has to be well controlled and analyzed.

1.2 Noise Microscopy

To date, noise studies were performed via spectrum analyzer, measuring total current noise from many noise sources in the channel of electronic devices. Noise data were statistically analyzed with multiple devices. [3] And, we couldn’t reveal specific locations and individual effects of noise sources. To solve these problems, our group developed a noise microscopy method. [3] Noise microscopy is the combined system of the C-AFM and a spectrum analyzer, which measures a nanoscale current and noise

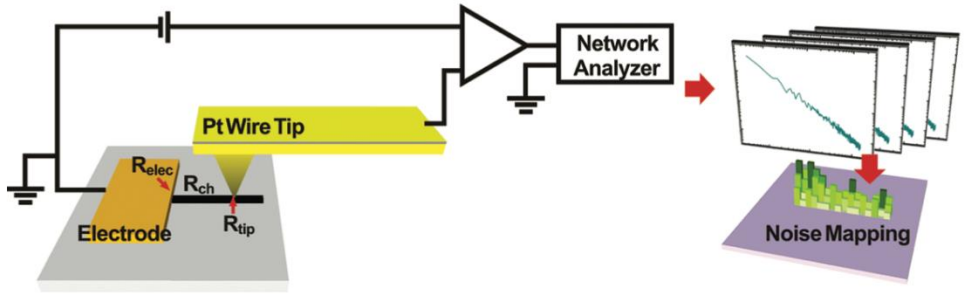

Fig. 1 Schematic diagram depicting a noise microscopy [3].

maps.

Figure 1 shows the schematic diagram for a noise microscopy based on conducting atomic force microscopy (C-AFM). Here, a conducting probe installed on C-AFM was directly contacted with the surface of a sample. While the tip scanned the sample, current and noise maps were simultaneously measured. Further, by analyzing these current and noise maps, we could calculate the map of localized noise source, that is, charge trap density. [4] Noise microscopy is a powerful tool for basic noise researches and advanced applications in many areas.

Chapter 2.

Noise Microscopy on an ITO Thin Film

2.1 Introduction

Indium tin oxide (ITO) is a highly n-doped semiconductor which has a low resistivity of ~ 10^{-4} Ω cm and a high mobility of ~ 1-10 cm^2 V^{-1} s^{-1}, with a high carrier concentration of 10^{20} - 10^{21} cm^{-3}. [5,6] The high conductivity of an ITO thin film is due to interstitial tin (Sn) dopants and oxygen vacancies from an In_2O_3 lattice. In the ITO lattice, when a Sn^{4+} located in an In^{3+} site, one free electron was generated. Also, since some oxygen atoms were absent in original sites, doubly charged oxygen vacancies introduced two electrons, and these free electrons were provided to the conduction band. [5,7,8] Further, an ITO thin film shows high optical transmittances (~ 80%) [9] in visible and NIR regions, which originates from a wide band gap of ~ 3.5 - 4.3eV [10]. Since ITO thin films have remarkable electrical and optical properties, ITO thin films have been extensively used as promising transparent conducting electrodes in many optoelectronic devices such as light emitting diodes (LEDs), organic photovoltaics (OPVs), solar cells, gas sensors, touch screen displays and so on. [7-9,11-13]

In applying ITO thin films as electrodes for optoelectronic devices, high electrical conductivity of ITO thin films is considered as most important factor determining the quality of ITO thin films. The

electrical properties of an ITO thin film were dependent on many factors including deposition conditions and post-treatments. [10,14-23] Among various treatments, an oxygen plasma treatment is the most commonly used because it immediately affects the surface of an ITO thin film, resulting in a high conductivity and homogeneous electrical activities. [8,15,24] Also, it has been reported that the improvement in the electrical performance of ITO films after the plasma treatment is related to various types of charge traps present in ITO thin films. [7,8,24-27]

Charge traps are deeply related not only in the electrical conductivities of ITO thin films but also in the generation of current-noise signals. Therefore, studying the correlation between electrical conductivities and noise signals can provide various important information for improving the performance of ITO thin films. However, it was difficult to identify a noise-generating-phenomenon by localized noise sources on the material. Because, the most commonly used noise measurement equipment like a spectrum analyzer doesn’t provide the local characteristics of measured devices. To solve the problem, our group developed a new noise source mapping equipment based on conducting atomic force microscope (c-AFM) for 2D device channels. Using this, we could directly visualize the microscopic distribution of noise sources in ITO thin films.

Herein, we report the nanoscale effects of charge trap activities in an oxygen plasma-treated ITO thin films. In this work, ITO thin films with and without an oxygen plasma treatment were scanned by a conducting probe that was in contact with the ITO surface. Then, current and noise maps of the ITO thin film were recorded through the probe. By analyzing measured data maps, we calculated a sheet conductance map and a localized charge trap distribution map of ITO thin films in nanoscale resolution. These maps show low sheet conductances and high density of charge traps in grain boundaries. Interestingly, the sheet conductance and the charge trap density had the scaling behavior of $G_s \propto N_{eff}^{-0.5}$, indicating diffusive charge transports through charge traps in the ITO thin film. Additionally, a sheet conductance increased, and a charge trap density decreased in the ITO thin film as the result of an oxygen plasma treatment. Furthermore, from the scaling relation of $G_s \propto N_{eff}^{0.5}$, we could identify that charge carriers flowed through the hopping state in some grain boundaries of O_2 plasma-treated ITO thin film. Since our method provides valuable insights into the nanoscale effects of charge transports and the activities of charge traps in the ITO thin films, it can be a useful tool for the development of optoelectronic devices based on ITO electrodes.

2.2 Experimental Setup

2.2.1 Sample Preparation

An ITO thin film was purchased from the Sigma Aldrich, Inc. (703192). The ITO thin film was rinsed successively by acetone, ethanol, and deionized water for 1 min each and dried with nitrogen blowing. Then, we deposited two Ti/Au electrodes (10/30 nm, the size of ~ 0.2 × 1.2 cm) onto the ITO thin film using a thermal evaporator with a shadow mask.

2.2.2 Noise Measurement

Fig. 2.1 shows the experimental setup of our current and noise measurement. For a measurement, a conducting platinum (Pt) probe (25Pt300B, Park Systems Inc.) installed in conducting atomic force microscopy (c-AFM) (XE-70, Park Systems Inc.) made a direct contact with the surface of an ITO thin film. During the measurement, a contact force between the conducting Pt probe and the ITO surface was maintained as 2μN , and the DC bias voltage of 0.06V was applied to the Ti/Au electrode using a function generator (DS345, Standard Research Systems). Here, the current signals through the Pt probe were measured and converted to voltage signals

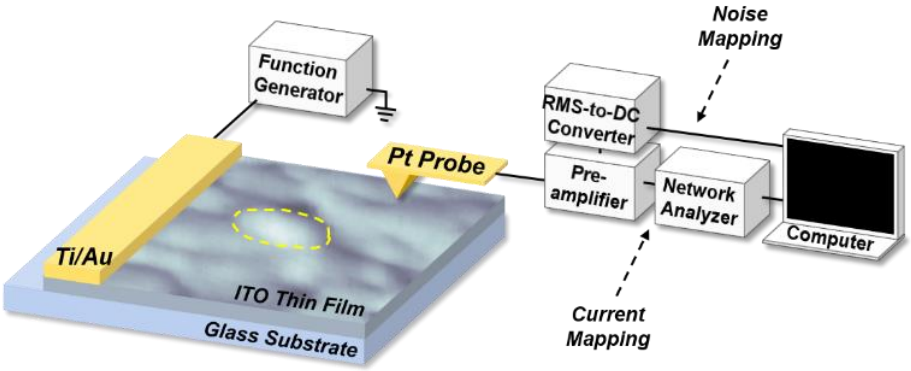

Fig. 2.1 Schematic diagram of a noise microscopy for an ITO thin film. Schematic diagram depicting the noise measurement setup for an ITO thin film on a glass substrate. The yellow dashed line indicates a grain in the ITO thin film. A conducting Pt probe installed on a c-AFM made a contact with the surface of the ITO thin film and scanned the ITO surface. Electrical current and noise maps were measured and analyzed to obtain sheet conductance and charge trap density maps.

by a low-noise preamplifier (SR570, Stanford Research Systems). Simultaneously, noise signals (the fluctuating component of an electrical current signal) were collected through a band-pass filter (6dB) in the preamplifier (SR570, Stanford Research Systems), and the RMS power of the measured noise signals were obtained using a homemade RMS-to-DC converter. The measured RMS noise power was divided by the bandwidth of the band-pass filter to estimate the absolute noise power spectral density (PSD). By scanning the probe on an ITO surface, high-resolution topography, current, and noise PSD maps could be acquired simultaneously. The measured maps were analyzed using a numerical method to obtain the maps of sheet conductance and charge trap density.

2.2.3 Oxygen Plasma Treatment

For the oxygen plasma treatment, an ITO thin film was exposed to the oxygen plasma produced by a radio frequency (RF) plasma generator (PDC-002, Harrick Plasma). We applied a RF power of 30W for 5 mins with the oxygen pressure of ~ 100 mTorr.

2.3 Results and Discussions

2.3.1 Optical and Electrical Properties of an ITO Thin Film

Fig. 2.2 (a) shows the transmittance curve of the ITO thin film in the visible region. We measured an optical transmittance using a UV-Vis/NIR spectrophotometer (V-770, JASCO). The spectrum shows that the ITO thin film exhibited a high optical transmittance over ~ 80%. And, the transmittance decreased at below ~ 350nm. It indicates that bandgap of the ITO thin film was ~ 3.5 eV. This energy level was similar to the reported bandgap of an ITO film. [28,29]

Fig. 2.2 (b) shows current-voltage (I-V) curve of an ITO thin film. A Keithley 4200-SCS semiconductor parameter analyzer was utilized to measure the current of an ITO thin film. A bias voltage was applied between two Ti/Au electrodes and swept from - 0.1 to 0.1V. Here, the length of the ITO channel was ~ 1.2cm, and the thickness of the ITO channel was ~ 150 nm. Measured current was proportional to the applied bias. The linear I-V curve indicates that ohmic contact between the ITO

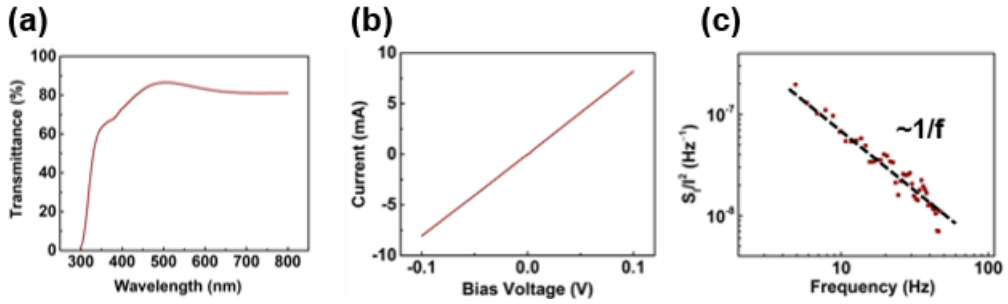

Fig. 2.2 Characterization of an ITO thin film. (a) The transmittance spectrum of the ITO thin film. (b) Current-voltage (I-V) curve measured on the film. (c) Current-normalized noise PSD (S_I/I^2) dependence on frequencies. 1/f noise behavior was observed in frequency range of 4 – 50 Hz.

channel and the electrode was formed, and contact resistances were negligible. From the slope of the I-V curve and the dimension of the ITO channel, we could calculate a sheet resistance value of ~ 130 Ω/sq, which is consistent with a previously measured value.

Fig. 2.2 (c) is the frequency dependence of a current-normalized noise PSD (S_I/I^2) spectrum on a log-log scale. A fast Fourier transform (FFT) network analyzer (SR770, Standard Research Systems) was utilized to measure a noise spectrum. Here, the same sample in Fig.2b was utilized. The bias voltage of 0.1V was applied to the Ti/Au electrode on the ITO thin film. And we measured a frequency dependence of noise spectrum between 5 and 50 Hz. The S_I/I^2 shows a 1/f behavior. In previous works, it was reported that when electrical noises were generated by a small number of trap states with a few variations of the trapping time of charge carriers, a noise PSD exhibited a

$1/f^2$ behavior. [25,30] On the other hand, in case of a numerous number of trap states with a various trapping time, a noise spectrum showed a 1/f behavior. [25,30] It indicates that there were various trap states with different trapping time in our ITO samples. And measured 1/f noise behavior was consistent with the 1/f noise characteristics of ITO thin films. [31]

2.3.2 Charge Traps Imaging of an ITO Thin Film

Fig. 2.3 (a) shows the AFM topography image of an untreated ITO thin film on a glass substrate. A grain boundary was marked by yellow dashed line, and a grain was the region inside the line. In the map, grains were distinguished from their boundaries. The topography map shows that the ITO thin film consisted of many grains whose sizes were ranged from 100 to 200 nm. And, the surface roughness was ~ 4 nm. Previous studies revealed that such surface roughness was due to a grain growth during a film deposition process. [18,22] Also, it was reported that the size of grains can be varied depending on the film deposition method, condition and the post treatment of an ITO thin film. [18,21-23]

Fig. 2.3 (b) is the current (I) map of the ITO thin film. For the current mapping, a DC bias voltage of 0.06V was applied to a Ti/Au electrode. Then, the current was measured while the Pt tip scanned over

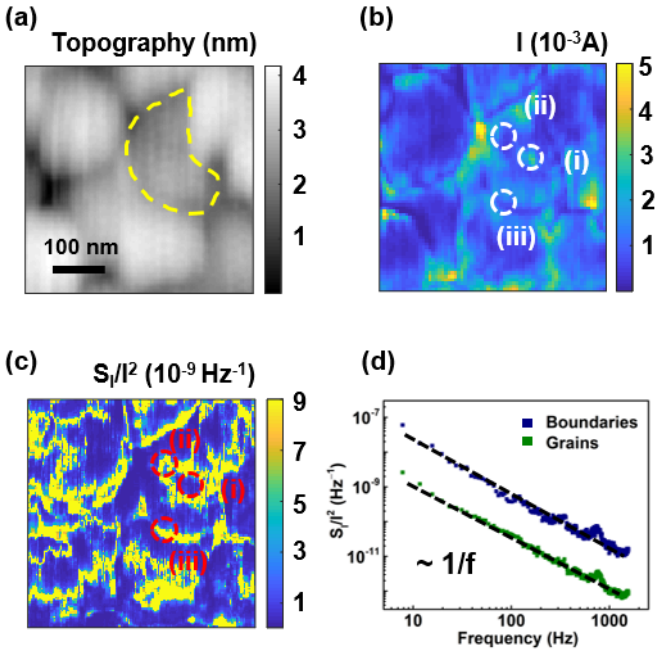

Fig. 2.3 Mapping of the ITO Thin film. (a) AFM topography image of the ITO thin film. The film was comprised of grains distinguished by grain boundaries. (b) Current (I) map of the film. Mark (i) and (ii) represented the region in a grain, and a mark (iii) represented a grain boundary. The bias voltage of 0.06V was applied to the film through a metal electrode. (c) Current-normalized noise PSD (S_I/I^2) map of the film at central frequency of 17.32Hz. (d) Current-normalized noise PSD (S_I/I^2) dependence on frequencies at each grains and grain boundaries.

the surface of the ITO film. The current value marked by (i) in a grain was ~ 2.9 × 10^{-3} A and the value marked by (ii) in the same grain was ~ 8.4 × 10^{-4} A. The current image shows a variation in current levels even in a same grain. Note that the current value of a grain boundary (marked by (iii)) was ~ 5.9 × 10^{-4} A, indicating that boundaries have lower current values than inside grains. Previous work showed that grain boundaries acted as barriers for carrier transport. [27,34] It was reported

that low current values in boundaries were owing to inter-granular amorphous phases, leading to the lattice mismatch. [32,33] This lattice mismatch could be attributed to many defects such as oxygen vacancies, oxygen interstitials, cation (In^{3+}, Sn^{4+}) vacancies, cation (In^{3+}, Sn^{4+}) interstitials. [7,12,16,32]

Fig. 2.3 (c) shows the map of a current-normalized noise PSD (S_I/I^2) at the central frequency of 17.32Hz. For the calculation of the current-normalized noise PSD (S_I/I^2) map, a noise PSD (S_I) map was measured simultaneously during the current (I) mapping. Then, the S_I/I^2 map was obtained from a S_I map divided by the square of the I map. The normalized noise PSD value of a grain boundary (marked by (iii), ~ 2.7 $\times$ 10^{-8} Hz^{-1}) was much higher than inside a grain (marked by (i), ~ 5.3 $\times$ 10^{-10} Hz^{-1}). It indicates that a large current noise was generated in grain boundaries. Previous works reported that defects were acted as charge traps for free carriers, generating electrical noises. [7,25,31,35] Therefore, presumably the high density of defects in grain boundaries made larger electrical noises than in grains. [31-33] Unlike previous researches, we can directly observe noise level differences between the grains and grain boundaries of ITO thin films using our noise mapping setup.

Fig. 2.3 (d) is the frequency dependence of the current-normalized noise PSD (S_I/I^2) which was measured at grain and boundary regions marked by (i) and (iii) respectively. A Pt probe installed on a c-AFM was placed on the specific location of grain or grain boundary. Then, we measured noise spectra in frequency range of 1 – 1.56 kHz using a fast Fourier transform (FFT) network analyzer (SR770, Standard Research Systems). During the measurement, a DC bias voltage of 0.06V was applied to the Ti/Au electrode. The spectra show typical 1/f behaviors. As reported previously, this result indicates that there were many trap states on grains and grain boundaries. [25,30] Also, the S_I/I^2 value of grain boundaries was higher than that inside grains at same frequency. It means that larger electrical noises were generated in grain

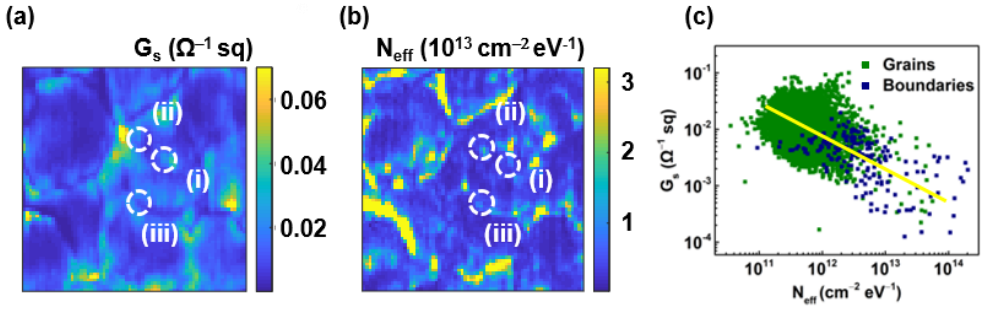

Fig. 2.4 Charge trap density imaging of the ITO thin film. (a) Sheet conductance (G_s) map for the ITO sample. (b) Charge trap density (N_{eff}) map for the film. (c) Scatter plot showing the relation between the G_s and N_{eff}. The slope of a yellow fitted line is ~ -0.5.

boundaries than inside grains of the ITO thin film. This result was coincident with the measured S_I/I^2 map (Fig.3c).

Fig. 2.4 (a) is the calculated sheet conductance (G_s) map of the ITO thin film. We calculated a sheet resistance map from the current map of an ITO thin film using repetitive computer calculations developed in our previous work. [30] Then, we could get the sheet conductance map by taking the reciprocal of the sheet resistance map. The G_s value in a boundary (marked by (iii)) was ~ 6.4 $\times$ 10^{-3} Ω^{-1} sq, while the grain region showed 3.9 $\times$ 10^{-2} Ω^{-1} sq (marked by (i)) and 9.3 $\times$ 10^{-3} Ω^{-1} sq (marked by (ii)). The result was consistent with the measured sheet conductance values of the ITO thin film (~ 10^{-2} Ω^{-1} sq). Although regions (i) and (ii) were in same grain, more conducting region of (i) showed ~ 4.2 times higher value than less conducting region of (ii). And the boundary (iii) had a ~ 1.5 times smaller value than the region (ii) inside the grain, much more the region (i). It was reported that the migration of charge carriers in the ITO thin film was attributed to the existence of Sn dopants and oxygen vacancies. [5,36,37] Presumably, local variations of Sn dopants and oxygen vacancies made sheet conductances different even in same grain. Also, the G_s values of boundaries much lower than those of grains could be resulted from

scattering centers located in boundaries. [10,33] Previous works reported that defects obstructed the flow of carriers in an ITO thin film by leading to the scattering of carriers, which could make low sheet conductance values in boundaries. [10,33]

Fig. 2.4 (b) shows the effective charge trap density (N_{eff}) map of an ITO thin film. In our previous work, we could calculate an effective charge trap density (N_{eff}) using a differential method. [25,26,30] The $N_{\mathbf{eff}}$ in a small area $\mathbf{\Delta x \Delta y}$ at (x,y) on an ITO thin film surface can be written as

$$\mathbf{N_{eff}(f,x,y) = \frac{(\Delta C)^2}{(I)^2}\frac{f}{kT} \times \frac{\Delta S_I(f,x,y)}{\Delta x \Delta y}}$$

where $\mathbf{\Delta C}$, **I**, **f**, **k**, **T**, **and** $\mathbf{\Delta S_I}$ are the number of charge carriers, a measured current, a frequency, a Boltzmann constant, a temperature, and a measured noise PSD in the small area $\mathbf{\Delta x \Delta y}$ in the ITO thin film, respectively. Using this equation, we calculated the effective charge trap density (N_{eff}) map of an ITO thin film from I (Fig. 2.3 (b)), S_I/I^2 (Fig. 2.3 (c)), and G_s (Fig. 2.4 (a)) maps. For the calculation, we used the value of ~ 1000 nm^2 as a $\mathbf{\Delta x \Delta y}$ which was the effective area of an ITO surface contacted with a conducting Pt probe. And for n, we used a reported carrier concentration value (~ 10^{14} cm^{-2}) in an ITO thin film. [7,36,40] Then, $\mathbf{\Delta C}$ could be calculated from $\Delta C = n\Delta x\Delta y$. The N_{eff} value on a boundary (marked by (iii)) was ~ 1.0 × 10^{12} cm^{-2} eV^{-1}, while N_{eff} values

on a grain were ~ 3.56 × 10^{11} cm^{-2} eV^{-1} (marked by (i)) and ~ 9.91 × 10^{11} cm^{-2} eV^{-1} (marked by (ii)). Previous works reported that the effective trap density of ITO thin films was ~ 10^{12} cm^{-2} eV^{-1}, which was consistent with our result. [39] Inside a grain, the density values of charge traps were much smaller than the value of the grain boundary region. The N_{eff} map shows that charge traps were not homogeneously distributed in the grain structures of the ITO thin film. Previously, it was reported that typical defects including oxygen interstitials, indium vacancies, and divalent Sn^{2+} acted as trap states in the ITO thin film. [5,7,9,40] These defects caused free electrons to be immobile in an ITO channel. [7] Also, high density of charge traps on grain boundaries plausibly due to the existence of many defects and a structure disordering. [41] Former research showed that the structure disordering in the boundary could be attributed to the segregation of Sn atoms into the In_2O_3 phases. [32] To date, previous studies indirectly reported that charge traps existed on the ITO thin film. [32,41] However, we could visualize the distribution of charge traps which make electrical noises in electronic devices.

Fig. 2.4 (c) is a scatter plot showing a relation between the sheet conductance (G_s) and the charge trap density (N_{eff}) of grains and grain boundaries in the ITO thin film on a log-log scale. Each data point was

obtained from a same pixel in the G_s and the corresponding N_{eff} maps. To distinguish the data points of grains and grain boundaries, data points for grains were expressed by green, and those for grain boundaries were navy. The plot shows that boundaries have smaller values of the G_s and higher values of the N_{eff} than grains. Interestingly, we observed that the G_s were inversely proportional to the root square of the N_{eff}, and this relation was written like as below.

$$\boldsymbol{G_s \propto \ N_{eff}^{-0.5}}$$

This result indicates that charge trap density (N_{eff}) can be a main factor in determining the sheet conductance (G_s) of an ITO thin film. In our previous work, we demonstrated that when charge carriers were scattered by the trapping of charge carriers (diffusive transport), this -0.5 correlation was observed. [25] Note that, it was reported that the main reasons of charge traps in the ITO films were oxygen interstitials, indium vacancies, and divalent Sn^{2+}. [5,7,9,40] These charge traps presumably obstructed the transport of charge carriers, making low sheet conductance at high density of charge traps in ITO thin films.

2.3.2 Effect of an Oxygen Plasma on Charge Trap Activities of an ITO Thin Film

We also investigated the effect of oxygen plasma treatment to ITO thin films (Figure 2.5). Fig. 2.5 (a) shows the sheet conductance (G_s) map of an O_2 plasma-treated ITO thin film. To obtain the G_s map from a measured current (I) map, we used the same iterative method in Fig.2.4 (a). The sheet conductance values of grain boundaries had a wide range from ~ 8.4×10^{-3} Ω^{-1} sq (marked by (iii)) to ~ 1.6×10^{-1} Ω^{-1} sq (marked by (i)), while the value of grains (marked by (ii)) was ~ 4.3×10^{-2} Ω^{-1} sq. Overall sheet conductance of the O_2 plasma-treated ITO increased to about twice, compared with an untreated ITO thin film. Additionally, it is worth noting that the G_s values of boundary regions were unusually increased, though still low values of the G_s were present. Previous research reported that oxygen plasma produced various kinds of oxygen ions and oxygen radicals such as O^+, O_2^+, and O^*. [43] The first plausible explanation of the increase of G_s is the injected oxygen ions (O^+, O_2^+) onto the surface of an ITO thin film, eliminating contaminants such as carbon atoms from the surface of the film. [15,42] Also, it was reported that oxygen radical (O^*) filled the sites of oxygen vacancies, which reduces the amount of oxygen vacancies. [43] As a

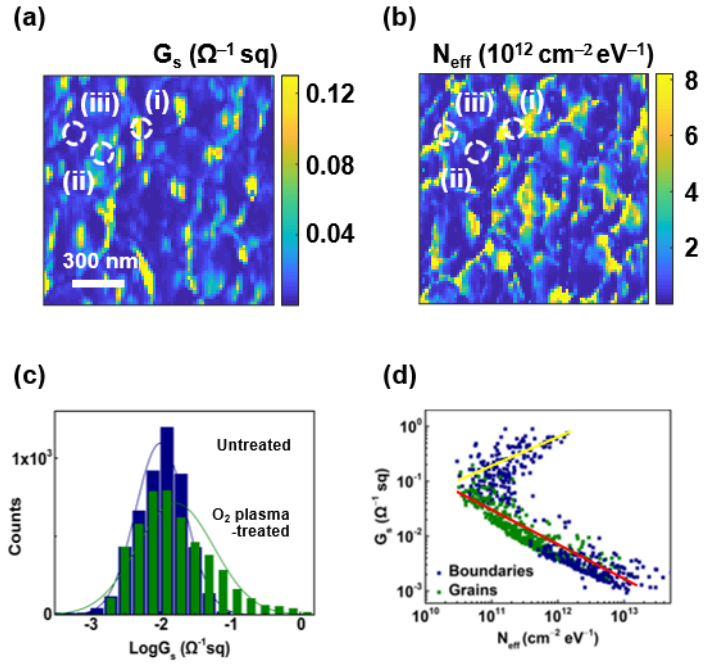

Fig. 2.5 Mapping the O_2 plasma-treated ITO thin film. (a) Sheet conductance (G_s) of the O_2 plasma-treated ITO thin film. Mark (i) and (iii) represented the region in a grain boundary, and a mark (ii) represented a grain. (b) Charge trap density (N_{eff}) of the ITO sample. (c) Statistical distribution of sheet conductance values in G_s maps in Fig. 2.5 (a). (d) Scatter plot showing the changes in the G_s and N_{eff} after being exposed to the oxygen plasma. The slope of a yellow fitted line is ~ 0.5, and the slope of a red fitted line is ~ -0.5.

result, the amount of crystalline In_2O_3 and SnO_2 phases plausibly increased. [42] Previous work showed that enhanced crystallization increased the conductivity of ITO thin films. [16] Although it was reported that an oxygen vacancy was the main source of the conductivity of an ITO thin film, high concentration of the oxygen vacancy in an ITO thin film could result in the scattering of charge carriers, thereby reducing the sheet conductance. [10,16] In this respect, an O_2 plasma-

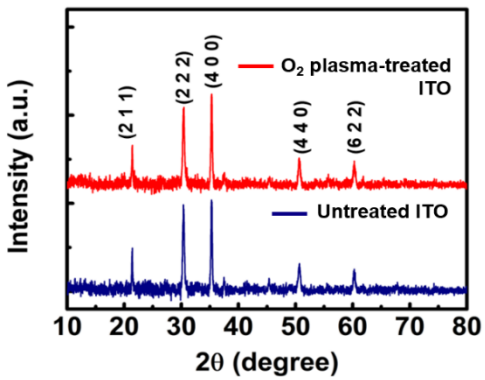

Fig. 2.6 XRD spectra of the untreated ITO and the O_2 plasma-treated ITO thin film.

treated ITO thin film could have a higher sheet conductance value than an untreated thin film. Furthermore, we identified structural changes after an oxygen plasma treatment to the ITO thin film. The XRD spectra (Fig. 2.6) implied that oxygen vacancies were replenished by the oxygen plasma. The XRD spectra shows that the intensity of peaks representing major planes of (211) and (222) increased after an oxygen plasma treatment. It indicated that the amounts of crystalline domain increased. Further, oxygen vacancies wouldn't be stable in a (222) plane, whereas preferentially located in a (400) plane. [10,44] So, the increased peak of the (222) plane and the decreased peak of the (400) plane could be attributed that oxygen vacancies were replenished by the oxygen plasma.

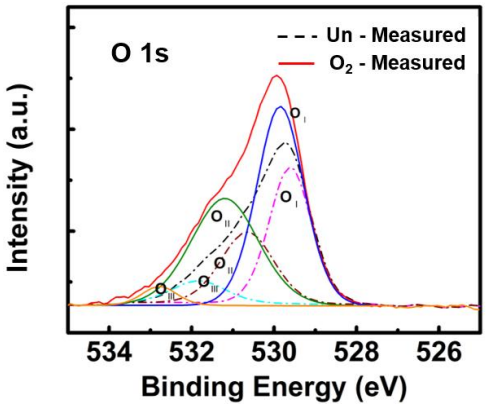

Fig. 2.7 XPS spectra (O 1s peak) of the untreated ITO thin film and the O_2 plasma-treated ITO thin film.

Also, to confirm the changes of a chemical composition in an ITO lattice, we additionally examined the ITO thin film by XPS measurement (Fig. 2.7). The O 1s peaks of the untreated ITO and the O_2 plasma-treated ITO thin film were de-convoluted to three components peaks: O_I, O_{II} and O_{III}. O_I and O_{II} peaks were related to an oxygen in an ITO lattice *without* and *with* oxygen vacancies, respectively. [45] O_{III} peak represented chemisorbed oxygen atoms onto a surface, namely oxygen contaminants. [45] XPS data shows that the amount of oxygen vacancies in an O_2 plasma-treated ITO lattice decreased, and more oxygen atoms were bonded with In and Sn compared with a untreated ITO. These results supported plausible explanation that more oxygen atoms were located in crystalline phases without oxygen vacancies as

the effect of oxygen plasma treatment. These results supported plausible explanation that more oxygen atoms were located in crystalline phases without oxygen vacancies as the effects of oxygen plasma treatment. Presumably, the effects of an oxygen plasma could remarkably appear in grain boundaries, since boundaries had more defects than grains. [10,32,33,41] Therefore, sheet conductance values in boundaries could be increased significantly. [32,41]

Fig. 2.5 (b) shows the effective charge trap density (N_{eff}) map of the O_2 plasma-treated ITO thin film. The map was calculated from measured current map and noise PSD map at 17.32Hz. The N_{eff} value of grains (marked by (ii)) was ~ 1.2×10^{11} cm^{-2} eV^{-1}, while boundary regions had a large variation of ~ 8.9×10^{10} cm^{-2} eV^{-1} (marked by (i)) and ~ 7.6×10^{11} cm^{-2} eV^{-1} (marked by (iii)) values. We could observe that the density of charge traps decreased by ~ 70% after an oxygen plasma treatment. Further, the charge trap densities of some boundaries were smaller than those of grains in the O_2 plasma-treated ITO thin film. Presumably, the oxygen radicals (O^*) filled up oxygen and cation vacancy sites, and the amount of charge traps was reduced. [42] In addition, charge traps on grain boundaries could be highly reacted with an oxygen plasma because of abundant defects in boundaries. So, the

amount of charge traps decreased significantly in some grain boundary regions.

Fig. 4c is the histogram of sheet conductance (G_s) of an untreated and an O_2 plasma-treated ITO thin films, which shows the statistical distribution of the G_s of ITO thin films on a log scale. The G_s values were extracted from Fig. 2.4 (a) (*Untreated ITO*) and Fig. 2.5 (a) (*O_2 plasma-treated ITO*) maps. Comparing with the sheet conductance values from the sheet conductance map (Fig. 2.4 (a) and Fig. 2.5 (a)), we could determine the *navy*- and *green*-colored histogram peak as the distribution of G_s values from the untreated and O_2 plasma-treated ITO thin films, respectively. Both histograms of the G_s were fitted to Gaussian distributions, indicating log-normal distributions. The shift of the histogram after an oxygen plasma treatment supported our observation as shown in Fig. 2.5 (a) where the sheet conductance increased compared with the value of an untreated ITO thin film (Fig.2.4 (a)). Previous works reported that log-normally distributed sheet conductance was due to the percolation characteristics. [26,46,47] Therefore, it is plausible that the grain structures of the ITO thin film could be considered as a percolation system with many charge traps.

To analyze a correlation between the sheet conductance (G_s) and the effective charge trap density (N_{eff}) of the O_2 plasma-treated ITO thin film more

in detail, we analyzed a scatter plot between the G_s and the N_{eff} (Fig. 2.5 (d)). Each data point was extracted from a same pixel in the G_s (Fig.2.5(a)) and the corresponding N_{eff} (Fig.2.5 (b)) maps. The data from grains and grain boundaries in maps were represented with *green*- and *navy*-colored squares, respectively. The distribution of data from grains of the oxygen plasma-treated ITO thin film was similar with that shown in Fig.2.4 (c). However, note that data points for boundaries were divided to two parts: (i) high G_s with low N_{eff} values and (ii) low G_s with high N_{eff} values. A positive correlation between the G_s and N_{eff} was observed in the first part (i), as indicated by a yellow line with the slope of ~ 0.5. The other part (ii) of grain boundaries and grain regions had a negative correlation indicated by a red fitted line with the slope of ~ -0.5. Hence, although oxygen plasma treatment decreased the density of charge traps distributed in the grain structures of the ITO thin film, remaining defects presumably could act as charge traps. So, the diffusive charge transports of charge carriers in the ITO thin film were maintained after the oxygen plasma treatment. This result is shown in the plot with a red fitted line, which is similar with the data distribution of the untreated ITO thin film (Fig.2.4 (c)). On the other hand, unique positive correlation between the G_s and the N_{eff} for grain boundary regions (i) could be attributed to hopping of charge carriers by localized states. With progressive oxygen plasma treatment to an ITO thin film, the density of charge traps significantly decreased. This oxygen plasma effect

could appear manifestly in grain boundary regions, since boundary had a high density of defects. So, it was plausible that charge traps did not disturb the charge trapping of carriers, and hopping conduction could dominate the charge transport in grain boundaries. In our previous works, authors verified that when charge carriers flowed through hopping states, a relation between the G_s and the N_{eff} was written like as below. [25]

$$G_s \propto N_{eff}^{\frac{1}{2}}$$

And this tendency was observed in our plot with a yellow fitted line. Our method allowed us to quantitatively map the activities of charge traps and provided important insights on nanoscale charge transport as a result of the oxygen plasma treatment on the ITO thin film.

3

Conclusions

We mapped the nanoscale distribution of charge trap activities in the grain structures of a O_2 plasma-treated ITO thin film. In this work, the electrical current and noise maps of an ITO thin film were recorded using a conducting probe installed in a conducting atomic force microscopy (c-AFM) while maintaining a contact with the surface of the ITO film. And, measured current and noise maps were utilized to obtain nanoscale sheet conductance and charge trap density maps in the ITO thin film. Our results show that boundaries exhibited a lower sheet conductance and a higher charge trap density than inside grains in the untreated ITO thin film. Interestingly, we observed that the sheet conductance and the charge trap density had the relation of $G_s \propto N_{eff}^{-0.5}$, indicating the diffusive charge transports where many defects acted as charge traps in the ITO thin film. In the O_2 plasma-treated ITO thin film, a sheet conductance increased to about twice and the density of charge traps decreased by ~ 70%, compared with the untreated ITO thin film. Interestingly, we could observe the scaling behavior of $G_s \propto N_{eff}^{0.5}$, indicating the hopping transport in some grain boundaries of the O_2 plasma-treated ITO thin film. Our work can be a powerful guideline for realizing the nanoscale activities of charge traps and the charge transport mechanism in the ITO thin film, and thus can be utilized to

basic noise studies for advanced optoelectronic devices based on an ITO electrode.

Chapter 4.

Abstract in Korean

초록

ITO 박막의 결정 구조에서 나노 스케일의 전하 트랩의 매핑에 관한 연구

전혜송

재료공학부

서울대학교 대학원

ITO 박막은 대표적인 투명 전극 재료로, 높은 전기전도도와 이동도를 가지며 가시광 영역에서 높은 빛 투과성을 띤다. 이러한 특성을 바탕으로 ITO 박막은 광전자 소자에 널리 사용되며, ITO 박막의 전기 전도도와 노이즈 특성은 이를 이용한 소자의 전체적인 전기적 특성을 결정한다. 한편, 전기적 전류 노이즈는 전류의 원치 않게 변동하는 전기적 신호로, 전자 장비의 전류 특성을 악화시킨다. 이 노이즈는 전자 장비의 수행력에 영향을 미치기 때문에 잘 제어해 주고 분석해야 한다.

본 논문에서는 전도성 원자 힘 현미경에 기반한 노이즈 현미경을 사용하여 ITO 박막의 결정 구조에서 나노 스케일의 해상도로 전하 트랩의 분포에 대해 논의할 것이다. 이 연구에서는 노이즈 현미경을 통해 ITO 박막의 결정 구조의 전류와 노이즈 맵을 얻었

다. 이를 이용해 ITO 박막에서의 면 전도도와 전하 트랩 밀도의 맵을 계산하였다. 그리고 이를 분석하여 ITO 박막에서의 면 전도도는 트랩 밀도에 큰 영향을 받는 것을 확인하였고, 전하가 트랩에 의해 이동함을 확인할 수 있었다. 추가적으로, 산소 분위기에서 ITO 박막에 플라즈마 처리를 하였을 때 면 전도도와 전하 트랩의 변화를 관찰하고 이를 분석해 전하 이동 메커니즘에 대해 연구하였다. 산소 플라즈마 처리를 하면 ITO 박막의 면 전도도가 증가하고, 트랩 밀도는 감소함을 확인하였다. 흥미롭게도, 결정 경계 부분에서는 특히 큰 변화가 있음을 알 수 있었는데, 이는 결정 경계 부분에 많은 결함이 집중되어 있어 산소 플라즈마 효과가 크게 나타났기 때문이라 유추할 수 있다. 또한, 이 부분에서 트랩이 전하 이동을 돕는 호핑 전도가 이루어 짐을 밝혔다.

본 연구는 ITO 박막에서 노이즈를 일으키는 전하 트랩의 활동도와 전하 이동 메커니즘을 밝힐 수 있는 유용한 정보를 제공해 준다. 또한, ITO 박막에 기초한 광전자 소자의 노이즈 연구에 활용될 수 있다.

주요어: 인듐주석산화물 박막, 전기적 노이즈, 전하 트랩, 원자 힘 현미경, 산소 플라즈마

학번: 2019-23053

5 References

[1] Y. Song, T. Lee, *Journal of Materials Chemistry C*, 2017, **5**, 7123-7141.

[2] A. A. Balandin, *Nature nanotechnology*, 2013, *8*(8), 549-555.

[3] H. Lee, D. Cho, S. Shekhar, J. Kim, J. Park, B. Hong, and S. Hong, *ACS nano*, 2016, **10**, 10135-10142.

[4] H. Lee, D. Cho, S. Shekhar, J. Kim, J. Park, B. H. Hong, and S. Hong, *Acs Nano*, 2016, **10**, 10135-10142.

[5] R. B. H. Tahar, T. Ban, Y. Ohya and Y. Takahashi, *Journal of Applied Physics*, 1998, **83**, 2631-2645.

[6] S. Ray, R. Banerjee, N. Basu, A. K. Batabyal and A. K. Barua, *Journal of Applied Physics*, 1983, **54**, 3497-3501.

[7] T. Omata, H. Fujiwara, S. Otsuka-Yao-Matsuo and N. Ono, *Appl. Phys. A*, 2000, **71**, 609–614.

[8] N. R. Armstrong, P. A. Veneman, E. Ratcliff, D. Placencia and M. Brumbach, *Acc Chem Res*, 2009, **42**, 1748-1757.

[9] H. Kim, C. M. Gilmore, A. Pique, J. S. Horwitz, H. Mattoussi, H. Murata, Z. H. Kafafi and D. B. Chrisey, *Journal of Applied Physics*, 1999, **86**, 6451-6461.

[10] M. Shakiba, A. Kosarian and E. Farshidi, *Journal of Materials Science-Materials in Electronics*, 2017, **28**, 787-797.

[11] N. G. Patel, P. D. Patel and V. S. Vaishnav, *Sensors and Actuators B-Chemical*, 2003, **96**, 180-189.

[12] T. Kuwabara, T. Nakayama, K. Uozumi, T. Yamaguchi and K. Takahashi, *Solar Energy Materials and Solar Cells*, 2008, **92**, 1476-1482.

[13] M. H. Ahn, E. S. Cho and S. J. Kwon, *Applied Surface Science*, 2011, **258**, 1242-1248.

[14] E. S. Lee, J. H. Choi and H. K. Baik, *Surf Coat Tech*, 2007, **201**, 4973-4978.

[15] Y. H. Liau, N. F. Scherer and K. Rhodes, *J Phys Chem B*, 2001, **105**, 3282-3288.

[16] L. Bárdoš and M. Libra, *Vacuum*, 1989, **39**, 33-36.

[17] H. Kim, J. S. Horwitz, G. Kushto, A. Pique, Z. H. Kafafi, C. M. Gilmore and D. B. Chrisey, *Journal of Applied Physics*, 2000, **88**, 6021-6025.

[18] Z. Ghorannevis, E. Akbarnejad and M. Ghoranneviss, *J Theor Appl Phys*, 2015, **9**, 285-290.

[19] M. Nisha, S. Anusha, A. Antony, R. Manoj and M. K. Jayaraj, *Applied Surface Science*, 2005, **252**, 1430–1435.

[20] F. E. Akkad, M. Marafi, A. Punnoose and G. Prabu, *phys. stat. sol. (a)*, 2000, **177**, 445.

[21] C. V. R. V. Kumar and A. Mansingh, *Journal of Applied Physics*, 1989, **65**, 1270-1280.

[22] Naser M. Ahmeda and F. A. S. , H.I. Abdulgafourb, Ahmed Alsadigc,d, A. Suliemane, M. Alkhoaryef, *Results in Physics*, 2019, **13**.

[23] J. W. Xu, Z. P. Yang, X. W. Zhang, H. Wang and H. R. Xu, *Journal of Materials Science-Materials in Electronics*, 2014, **25**, 710-716.

[24] C. C. Wu, C. I. Wu, J. C. Sturm and A. Kahn, *Appl Phys Lett*, 1997, **70**, 1348-1350.

[25] M. Yang, T. Y. Kim, T. Lee and S. Hong, *Sci Rep*, 2018, **8**, 15822.

[26] N. Shin, J. Kim, S. Shekhar, M. Yang and S. Hong, *Carbon*, 2019, **141**, 59-66.

[27] S. Shekhar, D. Cho, H. Lee, D. G. Cho and S. Hong, *Nanoscale*, 2016, **8**, 835-842.

[28] R. N. Chauhan, R. S. Anand and J. Kumar, *Thin Solid Films*, 2014, **556**, 253-259.

[29] Ş. Ţălu, S. Stach, D. Raoufi and F. Hosseinpanahi, *Electron. Mater. Lett.*, 2015, **11**, 749-757.

[30] H. Lee, D. Cho, S. Shekhar, J. Kim, J. Park, B. H. Hong and S. Hong, *Acs Nano*, 2016, **10**, 10135-10142.

[31] S. S. Yeh, W. M. Hsu, J. K. Lee, Y. J. Lee and J. J. Lin, *Appl Phys Lett*, 2013, **103**, 123118.

[32] I. A. Rauf and J. Yuan, *Materials Letters*, 1995, **25**, 217-222.

[33] D. Mergel and Z. Qiao, *J Phys D Appl Phys*, 2002, **35**, 794-801.

[34] H.-C. Lee and O. O. Park, *Vacuum*, 2004, **75**, 275–282.

[35] T. M. H. Nanto, S. Orito, and S. Takata, *Journal of Applied Physics*, 1988.

[36] J. Stotter, Y. Show, S. H. Wang and G. Swain, *Chem Mater*, 2005, **17**, 4880-4888.

[37] Y. Shigesato, S. Takaki and T. Haranoh, *Journal of Applied Physics*, 1992, **71**, 3356-3364.

[38] R. S. Datta, N. Syed, A. Zavabeti, A. Jannat, M. Mohiuddin, M. Rokunuzzaman, B. Y. Zhang, M. A. Rahman, P. Atkin, K. A. Messalea, M. B. Ghasemian, E. Della Gaspera, S. Bhattacharyya, M. S. Fuhrer, S. P. Russo, C. F. McConville, D. Esrafilzadeh, K. Kalantar-Zadeh and T. Daeneke, *Nat Electron*, 2020, **3**, 51-58.

[39] K. Ellmer and R. Mientus, *Thin Solid Films*, 2008, **516**.

[40] Q. Hou, J. Buckeridge, T. Lazauskas, D. Mora-Fonz, A. A. Sokol, S. M. Woodley and C. R. A. Catlow, *J Mater Chem C*, 2018, **6**, 12386-12395.

[41] J. H. Lee, Y. H. Kim, S. J. Ahn, T. H. Ha and H. S. Kim, *Mater Sci Eng B-Adv*, 2015, **199**, 37-41.

[42] I. Irfan, S. Graber, F. So and Y. L. Gao, *Org Electron*, 2012, **13**, 2028-2034.

[43] M. J. Liu and H. K. Kim, *Appl Phys Lett*, 2004, **84**, 173-175.

[44] S. I. Jun, T. E. McKnight, M. L. Simpson and P.D. Rack, *Thin Solid Films*, **476**, 1, 59-64.

[45] M. T. Dang, J. Lefebvre and J. D. Wuest, *ACS Sustainable Chem. Eng*., 2015, **3**, 12, 3373-3381.

[46] J. Kim, D. Hong, H. Lee, Y. Shin, S. Park, Y. Khang, M. Lee and S. Hong, 2013, **117**, 38, 19721-19728.

[47] M. Lee, M. Noah, J. Park, M. J. Seong, Y. K. Kwon and S. Hong, J. Phys. Chem. C, 2009, **5**,14, 1642-1648.